EUROPEAN ORGANIZATION FOR NUCLEAR RESEARCH

A MEASUREMENT OF THE $K^+ \to e^+\nu\gamma$ STRUCTURE DECAY*)

J. Heintze, G. Heinzelmann, P. Igo-Kemenes, R. Mundhenke,
H. Rieseberg, B. Schürlein**), H.W. Siebert, V. Soergel,
H. Stelzer+), K.-P. Streit and A.H. Walenta++)

Physikalisches Institut der Universität Heidelberg, Heidelberg, Germany
and
CERN, Geneva, Switzerland

ABSTRACT

The decay $K^+ \to e^+\nu\gamma$ has been investigated. For the structure-dependent part with positive γ helicity (SD_+) we obtain the branching ratio $\Gamma(SD_+)/\Gamma(K_{\mu 2}) = (2.16 \pm 0.37) \times 10^{-5}$ from 50 ± 3 events observed in the kinematical region $E_e \geq 235$ MeV, $E_\gamma > 45$ MeV and $\Theta_{e\gamma} > 140°$. For the corresponding part with negative γ helicity we obtain an upper limit $\Gamma(SD_-)/\Gamma(SD_+) < 11$ (90% confidence level) from the sample of electrons with energies 220 MeV $\leq E_e <$ 230 MeV and with no γ in the backward direction. This upper limit implies that the ratio of structure-dependent axial-vector and vector amplitudes lies outside the region $-1.8 < a_K/v_K < -0.54$.

For the decay $K^+ \to e^+\nu\nu\bar{\nu}$ the limit $\Gamma(K^+ \to e^+\nu\nu\bar{\nu})/\Gamma(K_{e2}) < 3.8$ (90% confidence level) was found.

Geneva - 3 October 1977
(Submitted to Nuclear Physics B)

---

*) Work supported by the Bundesministerium für Forschung und Technologie.

**) Now at IDAS GmbH, D 6250 Limburg, Kornmarkt 9, Germany.

+) Now at Gesellschaft für Schwerionenforschung, D 6100 Darmstadt, Germany.

++) Present address: Brookhaven National Laboratory, Upton, NY, USA.

1. INTRODUCTION

There are three decay modes of the charged K meson which give information about the structure of the kaon: $K_{\ell 3}$, $K_{\ell 4}$, and $K \to e\nu\gamma$.

As $K_{\ell 3}$ decay yields information on the vector form factor only, the rare decays K_{e4} and $K_{e\nu\gamma}$ are the only possibilities at present to study both axial-vector and vector form factors. These decays have comparable rates, but the signature of $K^+ \to e^+\nu\gamma$ is so ambiguous, compared to that of $K^+ \to \pi^+\pi^-e^+\nu$, that the experimental observation becomes much more difficult.

$K^+_{e\nu\gamma}$ decay has already been observed earlier [1]. We report here on an experiment with an improved apparatus, which resulted in reduced systematical errors.

There are two effects contributing to $K^+ \to e^+\nu\gamma$ decay:

- Internal bremsstrahlung (IB). This is a radiative correction to the ordinary K^+_{e2} decay, where the photon is emitted by the charged lepton (Fig. 1a). K^+_{e2} decay itself is mediated by the axial-vector current only.
- Structure decay (SD), where the photon is emitted from the K^+ decay vertex (Fig. 1b). Both axial-vector and vector currents may contribute. The corresponding amplitudes are denoted by a_K and v_K.

It has been shown by Neville [2] that the decay amplitude of SD can be separated into two non-interfering contributions, denoted by SD_+ and SD_-, which correspond to positive and negative γ helicities. The decay rates of SD_+ and SD_- are proportional to $|v_K + a_K|^2$ and $|v_K - a_K|^2$, respectively.

v_K and a_K have been calculated, assuming the K^* and K_A mesons as intermediate states (Fig. 1c). Various calculations of v_K agree to about 20%, whereas estimates for $\gamma_K = a_K/v_K$ yield less coherent results. The differences are mainly due to different methods of handling symmetry-breaking [3-6].

Owing to the fact that the kaon is spinless and e^+ and ν have fixed helicities (V-A interaction), SD_+ and SD_- have different angular correlations of the

decay particles, as indicated in Fig. 2. For SD_+ the γ is emitted preferentially antiparallel to the e^+, whereas for SD_- the γ is emitted preferentially antiparallel to the ν. Consequently, the electron spectrum for SD_+ is peaked at the maximum energy E_{max} = 247 MeV, whereas for SD_- it is peaked at $E_{max}/2$. An interchange of e^+ and ν corresponds to an interchange of SD_+ and SD_-.

For a quantitative discussion [2,7-9] the variables $x = 2E_\gamma/m_K$, $y = 2E_e/m_K$ and $z = 2E_\nu/m_K$ are used. The decay rate of SD is given by

$$\frac{d^2W}{dxdy} = \frac{G^2\, e^2\, m_K^7\, \sin^2\theta_C}{2^8\pi^3}\left[|v_K + a_K|^2\,(1-z)^2\,(1-x) + |v_K - a_K|^2\,(1-y)^2\,(1-x)\right] \tag{1a}$$

$$W_{SD_+} = \frac{G^2\, e^2\, m_K^7\, \sin^2\theta_C}{2^8\pi^3 \times 60}\,|v_K + a_K|^2 \tag{1b}$$

$$W_{SD_-} = \frac{G^2\, e^2\, m_K^7\, \sin^2\theta_C}{2^8\pi^3 \times 60}\,|v_K - a_K|^2\ . \tag{1c}$$

θ_C is the Cabibbo angle and G is the weak coupling constant.

The kinematical correlation between the $e^+\gamma$ angle and the e^+ and γ energies for $K_{e\nu\gamma}$ decay is shown in Fig. 3a. The intensity distributions for SD_+ and SD_- (Fig. 3b) show quantitatively what has already been qualitatively outlined above. Both SD_+ and SD_- produce a γ spectrum with an average energy of $^2/_3E_{max}$ = 165 MeV. The intensity distribution of IB in the $K_{e\nu\gamma}$ Dalitz plot is completely different, as shown in Fig. 3c. Interference terms between SD and IB are negligible.

In view of its small branching ratio [$\Gamma(SD)/\Gamma(K_{e3}) \approx 1/3000$], SD can only be measured near or above the maximum electron energy of K_{e3} decay, which is 228 MeV (y = 0.92). As the electron spectrum for SD_+ is peaked at its end-point energy, y = 1, about 20% of its electron spectrum can be observed above the K_{e3} spectrum. The separation between the decays K_{e2} and SD_+ can be achieved by detection of the γ-ray. As the $e\gamma$ angular correlation for SD_+ is strongly peaked backwards, it is possible to separate SD_+ from the bremsstrahlung tail of K_{e2}, where the $e\gamma$ angular correlation is strongly peaked in the forward direction.

In our experiment we identified SD_+ events in the kinematical region $y > 0.95$, $\Theta_{e\gamma} > 140°$ and $x > 0.18$, which is indicated in Fig. 3a. Here the fraction of events from SD_- is suppressed by a factor 400 compared to SD_+ and IB is expected to be three orders of magnitude smaller than SD_+.

We also searched for SD_- decay at electron energies below the K_{e2} line, suppressing the contribution from the decays K_{e3} and SD_+ by demanding that no γ was seen in the region $\Theta_{e\gamma} > 140°$. As the electron spectrum of SD_- is peaked at $E_{max}/2 = 123$ MeV, the observable fraction of SD_- events is much smaller than that of SD_+ decays. The kinematical region used for the search of SD_- decay is also indicated in Fig. 3a.

We emphasize that our experiment was mainly sensitive to SD_+.

2. APPARATUS

The experimental set-up, shown in Fig. 4, was used for a simultaneous study of $K_{\ell 3}$ [10], $K_{\ell 2}$ [11] and $K_{e\nu\gamma}$ decays. We mention here only those parts of the apparatus relevant to the $K_{e\nu\gamma}$ analysis. Kaons from a low-energy K^+ beam derived from the external proton beam of the CERN PS [12] are stopped and decay at rest in the target T. The momentum of the charged decay particles is measured in a magnetic spectrometer equipped with drift chambers D_1-D_6 [13] and counter hodoscopes H, A and B. Electrons are identified by the gas Čerenkov counter G. Opposite to the spectrometer the lead-glass counter L detects γ-rays with $\Theta_{e\gamma} > 140°$. The crucial points of the experiment are described below in more detail.

2.1 Target region and K-stop definition

For one stopping kaon, 40 pions passed the target. They were rejected by the plexiglas Čerenkov counter Č, and the slow K^+ were positively identified by a high threshold in the hodoscope E.

The target was made of 6 slabs of plastic scintillator, 0.5 cm thick each, and was inclined at 30° to the beam axis. Thus the energy loss of the decay particles in the target was small, whereas 70% of the incoming K^+ stopped inside the target. The pulse height was measured in each target slab individually and the trigger accepted K^+ as stopped if any target slab showed an amplitude which was at least four times bigger than that of the passing pions. On the average, 13,000 K^+ were stopped per PS pulse. The hodoscopes E and H defined the timings of the incoming K^+ and the outgoing decay particle, respectively.

To separate the decays SD_+ and K_{e3} on the basis of the electron momentum, it is essential that only K^+ decaying at rest are accepted. In the analysis we obtained a pure sample of such events by demanding that either the timing difference between counters E and H was bigger than 5 nsec ("late decays") or that the amplitudes in the target slabs showed the typical rapid increase of the energy loss along the path of a stopping particle. The corresponding amplitude cuts were derived from the amplitude behaviour of the late decays using the abundant number of K_{e3} and $K_{\mu 2}$ events. An additional cut in the amplitude of H rejected all events where the K^+ stopped in H.

After application of these conditions the fraction of K^+ decays in flight was less than 0.02% of all events. This limit was estimated by comparing the measured momentum distribution from $K_{\mu 2}$ decays which occurred during the first 5 nsec after a K stop with the one for late decays. The loss of good events owing to the different cuts was less than 15%, whereas the reduction of the data was about 35%.

The amplitude information of the target was also used to determine the slab in which the stop occurred. By this means, the energy loss of the decay particle in the target could be determined with a precision of ±0.5 MeV.

2.2 Momentum analysis

The spectrometer consisted of a magnet with a bending power of 5 kG • m, 3 drift chambers in front of the pole faces, and 3 drift chambers behind them.

All chambers allowed the determination of horizontal and vertical coordinates. The resolution was σ = 0.3 mm. The spectrometer covered a solid angle of $\Omega/4\pi$ = 1.6%.

The momentum of the decay particles was calculated using combinations of three chambers. If there were several combinations possible, the combination which was known to give the best resolution for $K_{\mu 2}$ decays was used. The comparison of the momenta calculated with different chamber combinations allowed the rejection of spurious tracks.

For the determination of the over-all momentum resolution, including the energy loss in the target, the μ's of 236 MeV/c from $K_{\mu 2}$ decay were used, for which a line with 5 MeV/c FWHM was obtained (Fig. 5).

2.3 Electron identification

The electron identification was based on the Čerenkov counter G, which is described in detail elsewhere [14].

The counter was filled with isobutane at atmospheric pressure. The Čerenkov light of the electrons was reflected by an approximately spherical mirror onto an array of 22 phototubes Philips 56 DVP 03. Electrons were identified by a coincidence of at least 2 phototubes. As a mirror we used an inflated aluminized mylar foil, 25 μ thick. Thus the thickness of the counter along the electron path corresponded to 4.3×10^{-3} radiation lengths.

After suitable timing and pulse-height cuts to reduce the background, the efficiency of G for electrons was $\varepsilon_G = 0.89 \pm 0.01$ and the probability of misidentifying muons from $K_{\mu 2}$ as electrons was 6×10^{-6}. This muon contamination was caused by random coincidences between the counter and $K_{\mu 2}$ decays and could be subtracted statistically.

2.4 γ-ray detection

γ-rays were detected by 3 wedge-shaped lead-glass blocks, each viewed by 3 phototubes 58 AVP. The blocks were stacked vertically as indicated in Fig. 4c. The thickness of the lead-glass in the direction perpendicular to the beam was equivalent to 7 radiation lengths. The pulse height was measured for each block separately and the timing was determined using the mixed signal of all blocks. The plastic scintillation counter V_L vetoed charged particles.

The counter was calibrated concurrently to the data taking with π^0 from $K_{\pi 2}$ and K_{e3} decays, for which the charged decay particle was detected in the spectrometer. From K_{e3} decay, electrons at the upper end of the momentum spectrum were used only, so that the π^0 momentum was known. The observed π^0 line width was 90% FWHM.

For SD_+ events with $y > 0.95$ the γ-detection efficiency was determined by Monte Carlo calculations, taking into account the combined effect of the energy cut and of the geometrical acceptance of the counter. The result was $\varepsilon_\gamma(SD_+) = 0.92 \pm 0.04$. The method was checked on $K_{\pi 2}$ and K_{e3} decays.

As the counter was placed very close to the beam axis, it had to sustain a high counting rate. In the analysis a 12 nsec wide timing gate was introduced to reduce random background. Because of this cut, events with an associated γ signal were lost if the γ signal was preceded by a random signal within the acceptance of the time digitizer. This loss, which was calibrated with K_{e3} and $K_{\pi 2}$ decays, reduced the detection efficiency by a factor $r = 0.76 \pm 0.01$.

For SD_+ candidates an amplitude corresponding to a γ energy of more than 45 MeV was required in the analysis. Since the average γ energy is 165 MeV, this cut was low enough to avoid large uncertainties in the detection efficiency.

2.5 Data taking

The data were taken concurrently for the three decay modes $K_{\ell 3}$ [10], $K_{\ell 2}$ [11] and $K_{e\nu\gamma}$. The trigger for $K_{e\nu\gamma}$ decay required a coincidence between the counters H, G, A, and B within 30 nsec after a K^+ stop, indicating that an electron from K^+ decay had passed the spectrometer. The γ counter was not included in the trigger. A fraction (1/256) of all K^+ decays was registered as a monitor and for calibration purposes. This sample contained mainly $K_{\mu 2}$ and $K_{\pi 2}$ decays.

3. EVENT ANALYSIS

3.1 $K^+ \to e^+\nu\gamma$ (SD_+)

From the events registered with the $K \to e\nu\gamma$ trigger those were selected which show a γ signal with $E > 45$ MeV in coincidence with the electron. Their electron momentum spectrum is shown in Fig. 6. At lower momenta ($p < 230$ MeV/c) it is dominated by the K_{e3} decay. The spectrum expected from K_{e3} decay was calculated taking into account internal bremsstrahlung, bremsstrahlung and Bhabha scattering in the target, and the measured momentum resolution. Good agreement is obtained (Fig. 6) with the experimental points below the K_{e3} end point at 228 MeV/c. At higher momenta the data show an excess of events over the calculated K_{e3} spectrum, extending up to 250 MeV/c.

The further analysis is restricted to the momentum region $p_e \geq 235$ MeV/c ($y > 0.95$) in which 57 events are contained. Besides $K_{e\nu\gamma}$ decay the following processes could give rise to $e\gamma$ coincidences in this region of electron momenta:

i) K_{e3} due to non-Gaussian tails in the decay resolution or to K^+ decays in flight. Both effects are taken into account in the calculated K_{e3} momentum spectrum, where the experimentally observed line shape from $K_{\mu 2}$ decay was inserted. We expect 4 ± 1 events from K_{e3} decay with measured momenta $p_e \geq 235$ MeV/c. Additional evidence for the absence of decays in flight is given by the decay time distribution of our sample (Fig. 7), which agrees with the K^+ lifetime.

ii) K_{e_3} decays where the high momentum positron is due to the π^0 either through a Dalitz pair or through an external pair (π^0 from K_{π_2} or K_{μ_3} decays fail to yield positrons with high enough momenta). Four positrons with $235\ \text{MeV/c} \leq p < 250\ \text{MeV/c}$ are expected from this source to fall into the solid angle of the spectrometer. From the decay kinematics it follows that they are accompanied by nearly antiparallel emitted e^+ from the K^+ decay and are therefore vetoed by V_L.

iii) K_{e_2} events with random γ signals. This source contributes 1 ± 1 events, as calculated from observed K_{μ_2} events with a random γ signal.

iv) K_{μ_2} events with random signals in both the γ counter and the gas Čerenkov counter. This contribution was evaluated from the timing distributions of both counters and found to be 2 ± 1 events.

The total estimated background sums up to 7 ± 3 events. We attribute therefore 50 ± 3 events to the decay $K^+ \to e^+\nu\gamma$. Since the contribution from SD_- is < 2 events, as will be shown below, they are essentially due to SD_+ decay.

This assignment is supported:

i) by the shape of the e^+ momentum spectrum; the dotted curve in Fig. 6, which is in good agreement with the data, was calculated for SD_+ kinematics and normalized to 50 events above $p = 235\ \text{MeV/c}$;

ii) by the shape of the pulse-height spectrum of the lead-glass counter, shown in Fig. 8a. This shape definitively rules out K_{e_3} decay and random coincidences as the origin of these events (cf. Figs. 8b and 8c). The poor energy resolution of the counter does not allow a positive identification, but the spectrum is in reasonable agreement with the expected shape from SD_+ decay.

We conclude that $N_{SD+} = 50 \pm 3$ events from $K_{e\nu\gamma}(SD_+)$ have been observed in this experiment. The number of $K_{\mu 2}$ decays corresponding to the sample of $K_{e\nu\gamma}$

events was evaluated from the monitor trigger sample to be $N_{K_{\mu 2}} = 2.203 \times 10^7$ events. The branching ratio for SD_+ decays with $y > 0.95$ is then given by

$$R(y > 0.95) = \frac{N_{SD_+}}{r\varepsilon_\gamma \varepsilon_G N_{K_{\mu 2}}} = (3.65 \pm 0.61) \times 10^{-6} .$$

The error comes mainly from the statistical uncertainty of N_{SD_+} (16%), a smaller contribution from ε_γ (4%). The fraction of SD_+ events with $y > 0.95$ turns out to be 0.169 ± 0.006, where the errors reflects the uncertainty in the momentum cut. The branching ratio for SD_+ decays obtained in this experiment is therefore

$$R = \frac{\Gamma(SD_+)}{\Gamma(K_{\mu 2})} = (2.16 \pm 0.37) \times 10^{-5} .$$

In Ref. 1, $\Gamma(SD_+)/\Gamma(K_{e2}) = 1.05^{+0.25}_{-0.30}$ is given. This yields with the branching ratio from Ref. 11 the combined result of both experiments:

$$\frac{\Gamma(SD_+)}{\Gamma(K_{\mu 2})} = (2.28 \pm 0.33) \times 10^{-5} .$$

3.2 $K^+ \to e^+ \nu\gamma$ (SD_-)

$K^+ \to e^+ \nu\gamma$ decays resulting from the SD_- term were searched for in the electron energy range $220 \leq E_e < 230$ MeV by demanding that no γ-ray was detected. In this energy range, γ-rays from K_{e3} and $K_{e\nu\gamma}$ (SD_+) are emitted in opposite direction to the electron and efficiently detected by the counter L, while γ-rays from $K_{e\nu\gamma}$ (SD_-) miss this counter with large probability (see Figs. 3a and 3b). At electron energies $E_e < 220$ MeV, the combined effects of the inefficiency of the counter L and of the rise of the K_{e3} spectrum prevent a search for $K_{e\nu\gamma}$ (SD_-). At electron energies $E_e > 230$ MeV, the $K_{e\nu\gamma}$ (SD_-) electron spectrum has fallen off so much that there is no hope to separate it from the K_{e2} bremsstrahlung tail and from misidentified $K_{\mu 2}$ muons.

The momentum spectrum of electrons which gave no signal in the γ counter L is shown in Fig. 9. The thin line represents the measured spectrum and the heavy line the spectrum after subtraction of random coincidences of $K_{\mu 2}$ events and signals in the gas Čerenkov counter G (see Ref. 11 for details of the background determination). Between 220 MeV/c and 230 MeV/c, 32 ± 1 electrons were observed, the error being due to the uncertainty in the background subtraction. There are three contributions expected from sources other than $K_{e\nu\gamma}$ (SD_-).

i) Owing to internal bremsstrahlung, external bremsstrahlung, and Bhabha scattering in the target, we expect 14 ± 2 electrons from K_{e2} decay, calculated from the observed number of events above 240 MeV/c.

ii) We expect contributions of > 9 events from K_{e3} decay and of ≥ 2 events from SD_+ decay, where the γ's were not seen in the γ counter L. These lower limits were obtained using values for the inefficiency $(1 - \varepsilon)$ of the counter L, which were calculated taking into account only the geometrical acceptance and the conversion probability: $1 - \varepsilon(K_{e3}) = 0.5\%$, $1 - \varepsilon(SD_+) = 4\%$.

iii) We expect ≥ 7 events from decay in flight of muons from $K_{\mu 2}$ decays, where the muon decayed between the target and the counter G.

These contributions sum up to ≥ 32 events. The observed event rate can therefore fully be accounted for by the three processes discussed. For an upper limit we obtain $N_{SD_-} < 9$ events (90% confidence level).

A fraction of 6.4×10^{-3} of all e^+ from SD_- decay would yield measured momenta between 220 MeV/c and 230 MeV/c in our apparatus, and at most 61% of these electrons would be vetoed by a γ-signal in the counter L.

For normalization to K_{e2} decay we used the high-energy part of the electron spectrum (Fig. 9), which contains 253 events in the momentum region between 240 and 255 MeV/c. These correspond to 68.4% of the total K_{e2} spectrum, taking into account the radiative tail from internal and external bremsstrahlung [11]. With the numbers given we obtain the following upper limits at the 90% confidence level:

$$\frac{\Gamma\left[K_{e\nu\gamma}(SD_-)\right]}{\Gamma(K_{e2})} < 10$$

$$\frac{\Gamma\left[K_{e\nu\gamma}(SD_-)\right]}{\Gamma(K \to all)} < 1.6 \times 10^{-4} .$$

From this number we calculated that the contribution of SD_- to our SD_+ sample is < 2 events, as mentioned above.

3.3 $K^+ \to e^+\nu\nu\bar{\nu}$

The upper limit for events in the momentum bite 220-230 MeV/c without a γ-ray can also be used to derive an upper limit on the decay mode $K^+ \to e^+\nu\nu\bar{\nu}$. Assuming the electron spectrum given by Bardin, Bilenky and Pontecorvo [15], which is nearly a phase space spectrum, we obtain

$$\frac{\Gamma(K_{e\nu\nu\bar{\nu}})}{\Gamma(K_{e2})} < 3.8 \qquad \text{(90\% confidence level)}$$

$$\frac{\Gamma(K_{e\nu\nu\bar{\nu}})}{\Gamma(K \to all)} < 6 \times 10^{-5} \quad \text{(90\% confidence level)} .$$

On the corresponding muonic decay mode an upper limit

$$\frac{\Gamma(K_{\mu\nu\nu\bar{\nu}})}{\Gamma(K \to all)} < 6 \times 10^{-6} \quad \text{(90\% confidence level)}$$

was reported [16].

4. CONCLUSIONS

From the branching ratios given in the preceding paragraphs, we obtain the following results for $K_{e\nu\gamma}$ structure decay:

$$\Gamma(SD_+) = (1172 \pm 170)\ \text{sec}^{-1}$$

$$\frac{\Gamma(SD_-)}{\Gamma(SD_+)} < 11 \text{ (90\% confidence level).}$$

From the measured decay rate $\Gamma(SD_+)$ we obtain with the aid of Eq. (1b) the value

$$\sin\theta_C \times m_K \times |v_K + a_K| = 0.0317 \pm 0.0023 \ .$$

The value of the Cabibbo angle derived from the K_{e3} decay rate, assuming $f_+(0) = 1$, is $\sin\theta_C = 0.212$. This yields

$$|v_K + a_K| = (0.149 \pm 0.011)\ m_K^{-1} \ .$$

The result on $\Gamma(SD_-)$ can be used to derive limits for the quantity $\gamma_K = a_K/v_K$. Using Eqs. (1b) and (1c), we obtain $|v_K - a_K| < \sqrt{11} \times |v_K + a_K|$. If T invariance is assumed, this inequality implies

$$\gamma_K < -1.86 \quad \text{or} \quad \gamma_K > -0.54 \ .$$

As already pointed out in the Introduction, v_K has been predicted assuming the $K^*(892)$ meson as intermediate state. The result is $v_K = 0.14 \times m_K^{-1}$, with an uncertainty of 20% arising from the relation between $K^*K\gamma$ and $\omega^0\pi^0\gamma$ couplings [6]. Estimates of the ratio γ_K, based on the assumption of the $K_A(1240\text{-}1400)$ meson as intermediate state, yield results between $|\gamma_K| = 0.05$ and $|\gamma_K| = 0.6$ [3-6].

Our result is compatible with all these theoretical predictions. The close numerical agreement of our value for $|v_K + a_K|$ with the predictions for v_K suggests, however, that the structure-dependent $K_{e\nu\gamma}$ decay is essentially a vector transition dominated by the $K^*(892)$ meson.

The experimental results resemble those obtained for the corresponding $\Delta S = 0$ decay $\pi \to e\nu\gamma$ [17,18], which also proceeds mainly by vector coupling.

Acknowledgements

We thank V. Roberto for his help in the experiment. We also thank our electronics engineer, H. Matsumura, and our technicians, L. Bonnefoy and J. Zimmer, for their efficient work in setting up and running the apparatus, M. Jouhet for her help in data handling, and E. Ehrbar and W. Farr and the institute workshops for the construction of the apparatus and the electronics.

REFERENCES

[1] K.S. Heard, J. Heintze, G. Heinzelmann, P. Igo-Kemenes, W. Kalbreier, E. Mittag, H. Rieseberg, B. Schürlein, H.W. Siebert, K.-P. Streit, A. Wagner and A.H. Walenta, Phys. Letters 55B (1975) 324.

[2] D.E. Neville, Phys. Rev. 124 (1961) 2037.

[3] H. Namaizawa, Progr. Theor. Phys. 39 (1968) 860.

[4] A.Q. Sarker, Phys. Rev. 173 (1968) 1749.

[5] R. Rockmore, Phys. Rev. 177 (1969) 2573.

[6] N.J. Carron and R.L. Schult, Phys. Rev. D 1 (1970) 3171.

[7] S.G. Brown and S.A. Bludman, Phys. Rev. 136 (1964) B1160.

[8] M.G. Smoes, Nuclear Phys. B20 (1970) 237.

[9] D.Yu. Bardin and S.M. Bilenkii, Yadernaya Fiz. 16 (1972) 557 [Transl. Sov. J. Nuclear Phys. 16 (1973) 311].

[10] J. Heintze, G. Heinzelmann, P. Igo-Kemenes, R. Mundhenke, H. Rieseberg, V. Roberto, B. Schürlein, H.W. Siebert, V. Soergel, H. Stelzer, K.-P. Streit, and A.H. Walenta, Measurement of the $(K^+ \to \pi^0\mu^+\nu)/(K^+ \to \pi^0 e^+\nu)$ branching ratio, to be published in Phys. Letters B.

[11] J. Heintze, G. Heinzelmann, P. Igo-Kemenes, R. Mundhenke, H. Rieseberg, B. Schürlein, H.W. Siebert, V. Soergel, H. Stelzer, K.-P. Streit and A.H. Walenta, Phys. Letters 60B (1976) 302.

[12] A. Bamberger, A. Colombo, J. Egger, U. Lynen, G. Petrucci, H. Piekarz, B. Povh, H.G. Ritter, G. Sepp and V. Soergel, CERN 72-2 (1972).

[13] A.H. Walenta, Nuclear Instrum. Methods 111 (1972) 467.

[14] J. Heintze, W. Kalbreier, H. Rieseberg, H.W. Siebert and K.-P. Streit, Nuclear Instrum. Methods 138 (1976) 641.

[15] D.Yu. Bardin, S.M. Bilenky and B. Pontecorvo, Phys. Letters 32B (1970) 121.

[16] G.D. Cable, R.H. Hildebrand, C.Y. Pang and R. Stiening, Phys. Letters 40B (1972) 699, Phys. Rev. D 8 (1973) 1989.

[17] P. Depommier, J. Heintze, C. Rubbia and V. Soergel, Phys. Letters 7 (1963) 285.

[18] A. Stetz, J. Carroll, D. Orthendahl, V. Perez-Mendez, G. Igo, N. Chirapatpimol and M.A. Nasser, Phys. Rev. Letters 33 (1974) 1455.

Figure captions

Fig. 1 : Diagrams contributing to $K_{e\nu\gamma}$ decay.

a) Internal bremsstrahlung. b) Structure decay. c) Structure decay with K^* and K_A as intermediate states.

Fig. 2 : Angular correlation and electron spectrum for a) SD_+, b) SD_-.

Fig. 3 : $K_{e\nu\gamma}$ Dalitz plot. $x = 2E_\gamma/m_K$, $y = 2E_e/m_K$.

a) $e^+\gamma$ opening angles. The shaded regions indicate the kinematical regions used for SD_+ ($y > 0.95$) and SD_- ($0.89 < y < 0.93$) measurements.

b) Contours for the SD_+ term (solid lines) and for the SD_- term (dashed line).

c) Contours for inner bremsstrahlung term.

Fig. 4 : Apparatus. a) Total view. b) Detailed view of target region; c) View of target region along the beam axis. K^+: incoming K^+ beam. $\check{C}$: plexiglas Čerenkov counter. E, H, A, B, C: scintillation counter hodoscopes. T: scintillator target. D_1-D_6: drift chambers. L: lead-glass γ-counter. V_L, V_G: veto scintillation counters. G: gas Čerenkov counter; the location of its phototubes is denoted by PM. NaI: 18 NaI counters $17 \times 17 \times 24$ cm^3, nine above and nine below drawing plane. P: 20 lead-glass counters $17 \times 17 \times 35$ cm^3, ten above and ten below drawing plane. The pole face of the bending magnet is indicated.

Fig. 5 : Observed muon line from $K_{\mu 2}$ decays.

Fig. 6 : Observed momentum spectrum of electrons with a signal in the γ counter. Dashed curve: calculated K_{e3} spectrum. Dotted curve: calculated SD_+ spectrum. Solid curve: sum of calculated K_{e3} and SD_+ spectra.

Fig. 7 : Observed decay time spectrum of $K_{e\nu\gamma}$ candidates. Dashed line : time spectrum after correction of loss due to K-stop condition. Smooth curve: expected K^+ decay-time distribution.

Fig. 8 : Measured γ-energy spectra. a) $K_{e\nu\gamma}$ candidates. b) K_{e_3} decays with $p_e \geq 220$ MeV/c. The spike at 240 analogue-to-digital converter (ADC) channels was produced by events where one of the three ADC units was set to the overflow channel. c) γ signals observed in random coincidences with K_{μ_2} decays.

Fig. 9 : Momentum spectrum of electrons without a coincident γ signal. Thin histogram: all events. Thick histogram: events after subtraction of random background. Smooth curve: calculated K_{e_2} line.

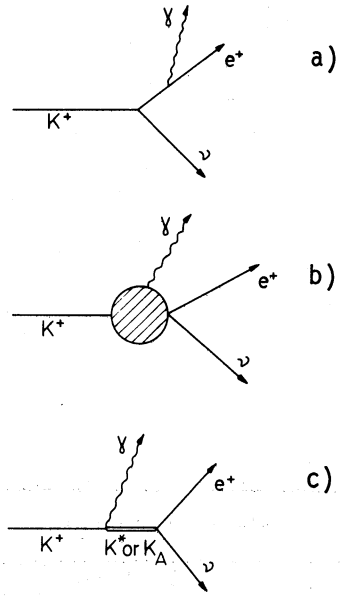
γ
e+
a)
K+
ν
γ
e+
b)
K+
ν
γ
e+
c)
K+
K* or K_A
ν

Fig. 1

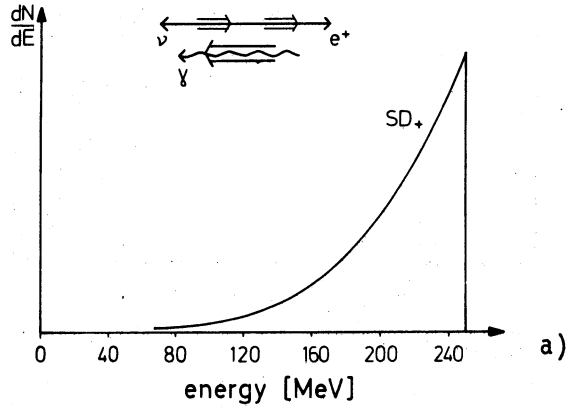
dN/dE
ν
e+
γ
SD+
0
40
80
120
160
200
240
a)
energy [MeV]

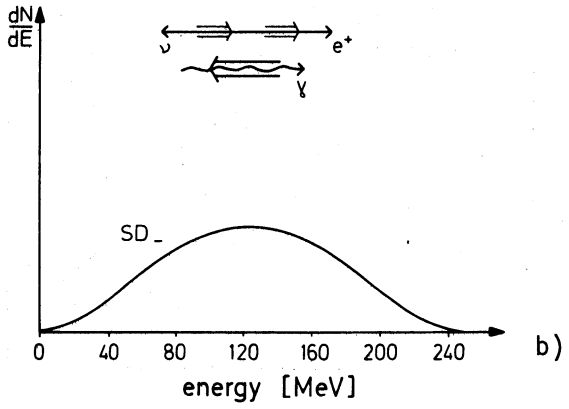
dN/dE
ν
e+
γ
SD-
0
40
80
120
160
200
240
b)
energy [MeV]

Fig. 2

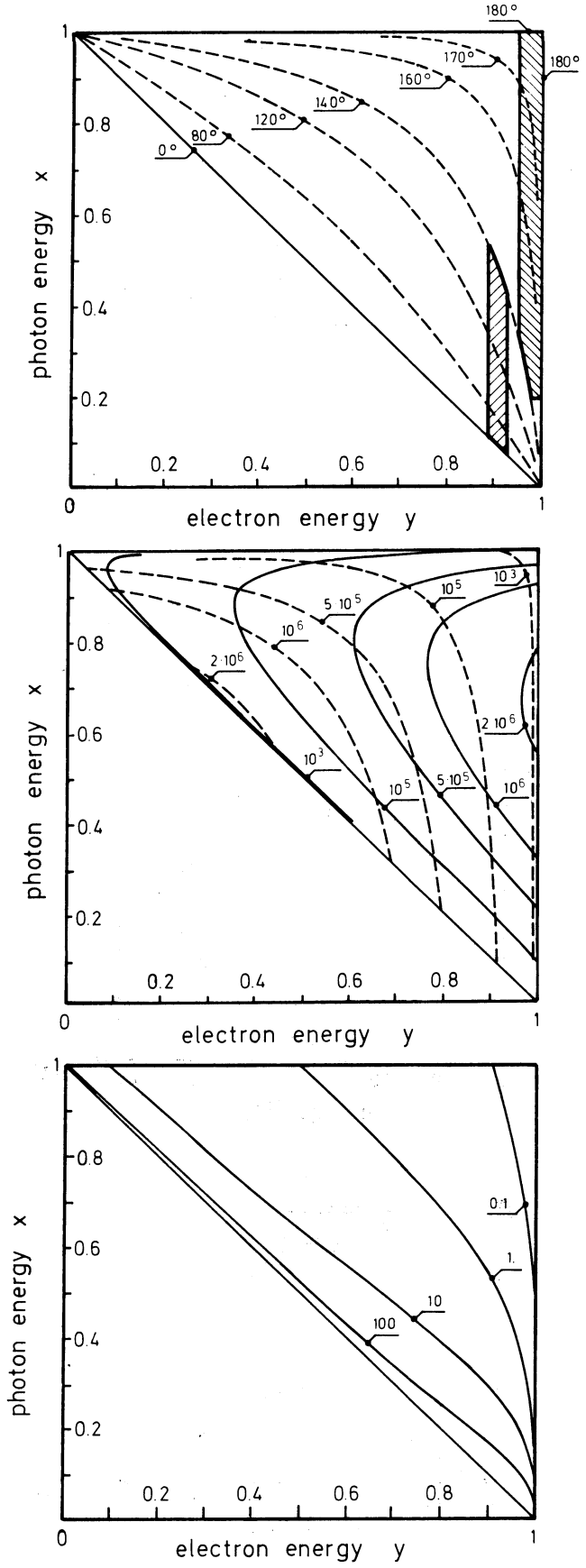
a)
b)
c)
photon energy x
electron energy y
0
0.2
0.4
0.6
0.8
1
180°
170°
160°
140°
120°
80°
0°
10³
5·10⁵
10⁵
10⁶
2·10⁶
0.1
1.
10
100

Fig. 3

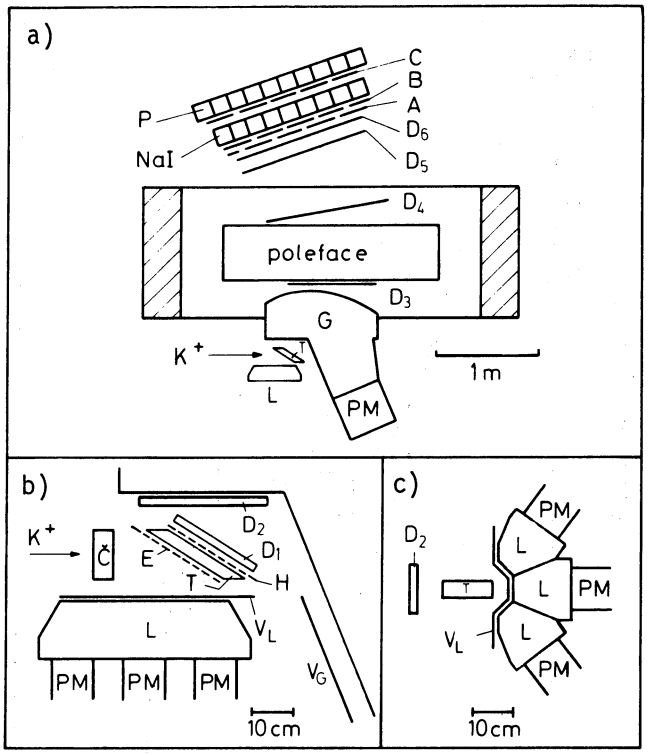
a)
C
B
A
P
D6
NaI
D5
D4
poleface
D3
G
K+
T
L
PM
1m
b)
D2
K+
Č
E
D1
T
H
L
VL
PM
PM
PM
VG
10cm
c)
PM
D2
L
T
L
PM
VL
L
PM
10cm

Fig. 4

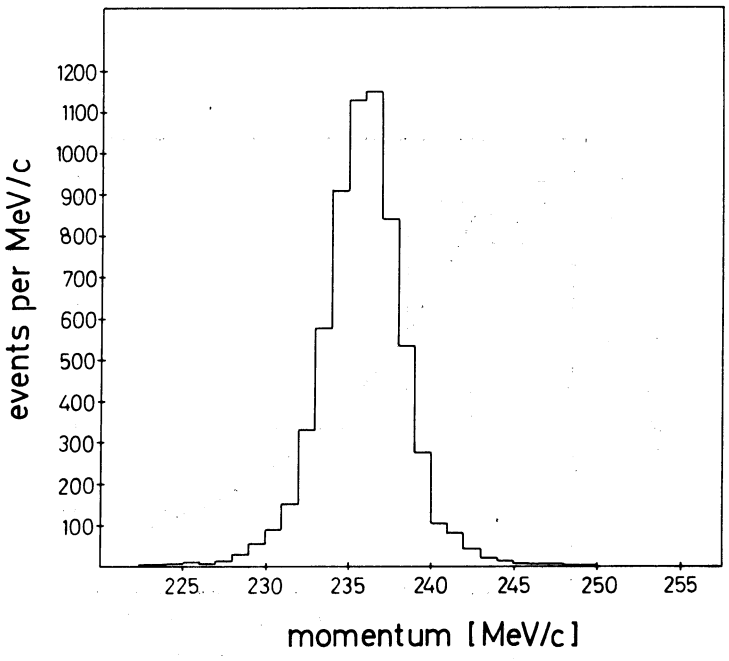
events per MeV/c
1200
1100
1000
900
800
700
600
500
400
300
200
100
225
230
235
240
245
250
255
momentum [MeV/c]

Fig. 5

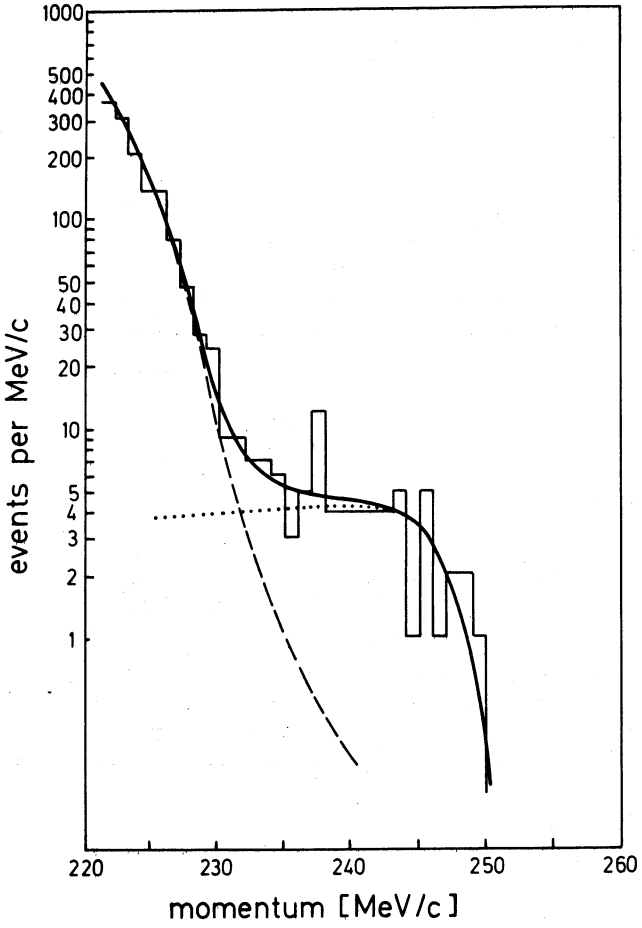
1000
500
400
300
200
100
50
40
30
20
10
5
4
3
2
1
events per MeV/c
220
230
240
250
260
momentum [MeV/c]

Fig. 6

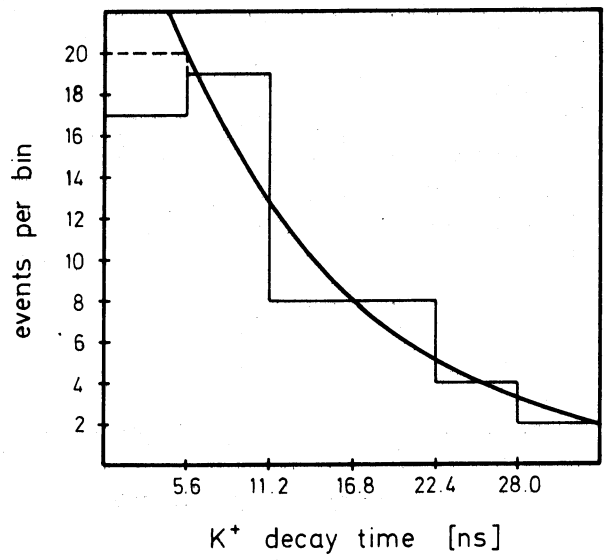
20
18
16
14
12
10
8
6
4
2
events per bin
5.6
11.2
16.8
22.4
28.0
K+ decay time [ns]

Fig. 7

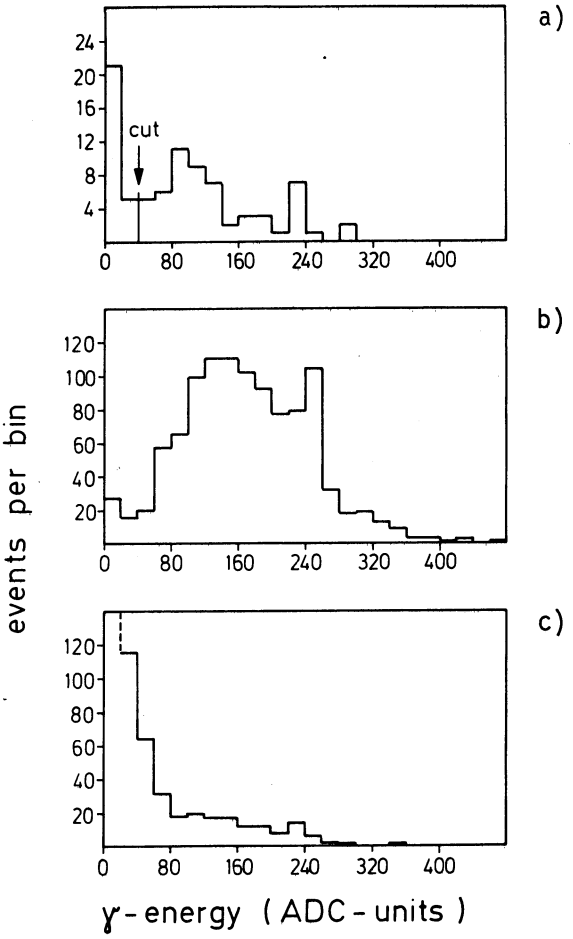
a)
b)
c)
cut
events per bin
γ-energy (ADC-units)

Fig. 8

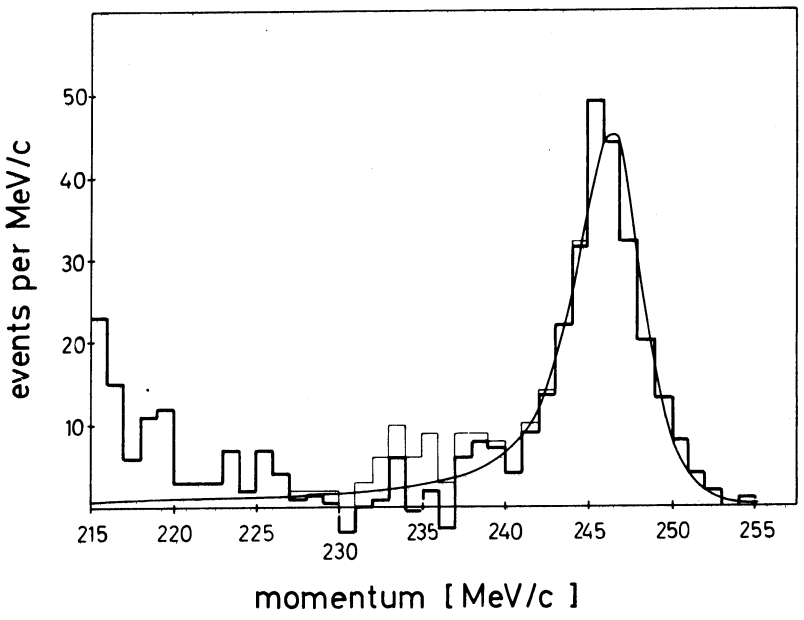
events per MeV/c
momentum [MeV/c]

Fig. 9